Improving Orbital Angular Momentum Mode Utilization With Mode Switching Periodically in Radar Forward-Looking Imaging

Yixin Wei, Gaofeng Shu, *Member, IEEE*, and Ning Li, *Member, IEEE*

***Abstract*—The infinity and orthogonality of the orbital angular momentum (OAM) of vortex electromagnetic waves (VEMWs) provide a new degree of freedom for the modulation of information. The VEMW generated by the uniform circular array (UCA) exhibits the characteristics of the Bessel function in terms of amplitude, and there is a null amplitude region in the beam center. This characteristic is particularly obvious when the array radius is small. In practical applications, it is usually necessary to switch OAM mode to ensure the richness of the received information. This leads to a sudden drop in radiation energy when switching OAM modes, and the OAM mode cannot be fully utilized. To address this issue, this letter proposes an OAM mode switching method based on the characteristics of the intersection of the adjacent-order Bessel functions for radar forward-looking imaging. Meanwhile, this letter introduces OAM mode repetition frequency (OMRF) to indicate the "speed" of switching OAM mode. Finally, through the application in the field of forward-looking radar imaging, it is proved that the method proposed in this letter can effectively improve the OAM mode utilization rate and anti-noise ability.**

***Index Terms*—Uniform circular array (UCA), Bessel functions, orbital angular momentum (OAM) mode switching method, radar imaging.**

I. Introduction

ORBITAL angular momentum (OAM) provides a new degree of freedom for information transmission [1]. Electromagnetic waves carrying OAM are vortex electromagnetic waves (VEMWs), which have a spiral phase structure and its wavefronts rotate along the beam axis in space [1], [2]. The infinity and orthogonality of the OAM of VEMWs make them have great potential in many fields [3].

So far, many methods have been developed to generate VEMWs, including spiral phase plates [4], discrete dielectric lenses [5], three-dimensional spiral antennas [6], and metasurfaces [7]. However, these methods are usually limited to a single OAM mode for a given structure. In order to employ multiple different modes of the OAM beams, uniform circular array (UCA) is mostly used to generate VEMWs [8].

Received 8 May 2025; revised 22 July 2025; accepted 24 July 2025. Date of publication 29 July 2025; date of current version 12 August 2025. This work was supported by the Natural Science Foundation of Henan under Grant 242300421170. The associate editor coordinating the review of this article and approving it for publication was Prof. Tirza Routtenberg. *(Corresponding author: Gaofeng Shu.)*

The authors are with the School of Computer and Information Engineering, Henan University, Kaifeng 475004, China, also with the Henan Key Laboratory of Big Data Analysis and Processing, Henan University, Kaifeng 475004, China, and also with the Henan Province Engineering Research Center of Spatial Information Processing, Henan University, Kaifeng 475004, China (e-mail: gaofeng.shu@henu.edu.cn).

Digital Object Identifier 10.1109/LSP.2025.3593646

The VEMW generated by UCA is modulated by the Bessel function in terms of amplitude [9]. The center of the non-zero-order Bessel function is null, which is inevitable, and as the radius of the UCA decreases or the OAM mode increases, the null spreads [10]. In the application field of VEMWs, a large OAM mode is often used, which will cause the radiation energy to be greatly weakened when the OAM mode is switched in a given direction.

To address this problem, existing applications are mostly based on a larger array radius [11], [12], [13]. This can reduce the impact of energy drops when switching OAM modes, but a larger radius means greater system complexity and increased cost, and this solution still cannot solve the problem that the OAM mode energy cannot be fully utilized when switching OAM modes.

In the field of radar imaging, researchers have proposed many methods to deal with the energy drop problem when switching OAM modes. The core idea of these methods is to adjust the main lobes of different OAM modes to align them with the region of interest (ROI). For example, in [11], Qu et al. proposed an imaging method based on uniform concentric circular arrays. Yuan et al. proposed a method to use phased array beam steering technology to align the main lobe of each OAM mode with the ROI [14]. However, these methods cannot be applied to platform motion scenarios.

To address the energy drop challenge when switching OAM modes, this letter analyzes the intersection of adjacent-order Bessel functions through numerical simulation. On this basis, this letter introduces a concept of OAM mode repetition frequency (OMRF) and proposes an OAM mode switching method. Finally, the proposed method is applied to radar forward-looking imaging. The simulation results verified that the proposed method can effectively improve energy utilization and signal-to-noise (SNR) of the images.

The rest of this letter is organized as follows. In Section II, the properties of the intersections of adjacent-order Bessel functions are analyzed through numerical simulation. In Section III, an OAM mode switching method is proposed and applied to radar forward-looking imaging. The superiority of this OAM mode switching method is verified through simulation results. The last section is the conclusion.

II. Adjacent-Order Bessel Functions Properties

A. The Amplitude Pattern Generated by UCA

Using UCA to generate VEMWs [2], N identical electric dipoles are evenly spaced along a circular ring with a radius of a.

To generate VEMWs with an OAM mode of order l, the dipoles are excited with the same amplitude and incrementing phase $\varphi_n = 2\pi l(n-1)/N$, $n = 1, 2, \ldots, N$, where n represents the index of the array element [2]. To simplify analysis, an OAM beam generated by the combination of scalar monochromatic fields with frequency ω in free space can be expressed as

$$F(l, \mathbf{r}, \omega) = \int_V G(\mathbf{r}, \mathbf{r}', \omega) s(\mathbf{r}') d\mathbf{r}' \tag{1}$$

where $G(\mathbf{r}, \mathbf{r}', \omega) = e^{-jk|\mathbf{r}-\mathbf{r}'|}/(4\pi|\mathbf{r}-\mathbf{r}'|)$ is the Green function, $k = \omega/c$ is the wave number, $s(\mathbf{r}')$ represents the discrete sampling of the phase-weighted array element [2]

$$s(\mathbf{r}') = \sum_{n=0}^{N-1} e^{-j\varphi_n} \delta(\mathbf{r} - \mathbf{r}') \tag{2}$$

where $\delta(\mathbf{r} - \mathbf{r}')$ represents the discrete sampling of the array element according to position.

Therefore, when the number of array elements N is large enough, the analytical expression of the generated VEMW can be expressed as [2]

$$U(l, \theta, \varphi) \approx N j^l e^{-jl\varphi} J_l(ka \sin\theta) \tag{3}$$

where $J_l(\cdot)$ represents the Bessel function of the first kind of l-th order.

To ignore the frequency effect, the radius a is replaced by the electrical size radius $\bar{a} = a/\lambda$, and therefore $ka = 2\pi\bar{a}$. From the properties of Bessel function [15], the amplitude of the l order Bessel function is smaller than that of the $l-1$ order function before the first non-zero intersection of the l-th and $l-1$-th order Bessel functions. Therefore, the following relationship can be obtained

$$\begin{aligned} &J_{l-1}(2\bar{a}\pi \sin\theta) > J_l(2\bar{a}\pi \sin\theta) \\ &\text{subject to} \quad |\theta| < |\theta_{l-1,l}| \end{aligned} \tag{4}$$

where $\theta_{l-1,l}$ represents the first non-zero intersection point of the adjacent-order Bessel function.

During the relative motion between the antenna and the target, the elevation angle changes, which causes most of the mode energy to be wasted when switching between different OAM modes to illuminate the target.

B. Property of the Adjacent-Order Bessel Functions

The Bessel function has the following expansion as $x \to \infty$ with l fixed.

$$J_l(x) \approx \sqrt{\frac{2}{\pi x}} \cos\left[x - \frac{(2l+1)\pi}{4}\right] \tag{5}$$

where $x = 2\pi\bar{a}\sin\theta$.

Let $J_l(x) = J_{l+1}(x)$, and we obtained

$$\cos\left[x - \frac{(2l+1)\pi}{4}\right] = \cos\left[x - \frac{(2l+3)\pi}{4}\right] \tag{6}$$

we can find that

$$x = \left(\frac{l}{2} + \frac{1}{2} + n\right)\pi \tag{7}$$

where n is any positive integer.

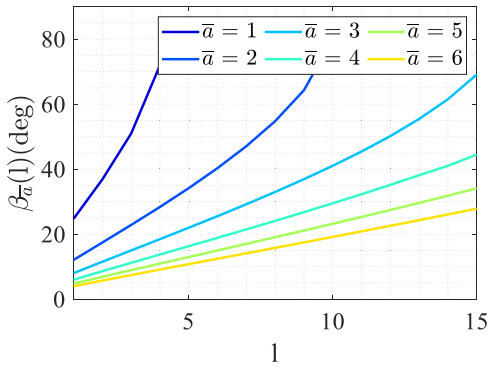

Fig. 1. Intersection points of adjacent-order Bessel functions.

From (7), it can be seen that as $x \to \infty$, the intersection of adjacent-order of the Bessel function satisfies a linearly varying relation with respect to order l, and the following relationship can be obtained

$$\theta = \arcsin\left(\frac{l+1+2n}{4\bar{a}}\right) \tag{8}$$

For different electrical size radii $\bar{a}$, the value of the adjacent order Bessel function first non-zero intersection point will also change. To investigate the properties of these intersection points, we get the following equation

$$\beta_{\bar{a}}(l) = \arg\min_{\theta} |J_l(2\bar{a}\pi \sin\theta) - J_{l-1}(2\bar{a}\pi \sin\theta)| \tag{9}$$

where $\beta_{\bar{a}}(l)$ denotes the θ value of the first non-zero intersection point between J_l and J_{l-1}. According to (9) and (8), we can get

$$\beta_{\bar{a}}(l) = \theta_l^{\bar{a}} \approx \frac{l+1+2n}{4\bar{a}} \tag{10}$$

Fig. 1 shows the intersection values for different $\bar{a}$. It can be observed that with a fixed $\bar{a}$, the intersection point $\beta_n(l)$ of the adjacent-order Bessel function changes linearly, which helps to provide a new way of OAM mode switching for improving energy utilization. The difference between the value computed through (9) and the value computed through (7) is very small, and as $x \to \infty$, the linear property of the intersection is still used when x is general, but a correction term needs to be included

$$x = \frac{\pi}{2}(l+1+2n) + \epsilon(l, n) \tag{11}$$

where $\epsilon(l, n)$ is a small correction related to l and n.

To better design the OAM mode switching method, it is necessary to calculate the value of the intersection interval

$$\alpha_{\bar{a}}(l) = \Delta\beta_{\bar{a}}(l) = \beta_{\bar{a}}(l) - \beta_{\bar{a}}(l-1) = \frac{1}{4\bar{a}} \tag{12}$$

From (12), the first non-zero intersection interval between the adjacent order Bessel functions of different electric radii $\bar{a}$ is inversely proportional to the electric radii $\bar{a}$, that is

$$\frac{\alpha_{\bar{a}_1}(l)}{\alpha_{\bar{a}_2}(l)} = \frac{\bar{a}_2}{\bar{a}_1} \tag{13}$$

Furthermore, we obtained a conclusion similar to that of (13) through numerical simulation

$$\frac{\text{mean}(\alpha_{\bar{a}_1}(l))}{\text{mean}(\alpha_{\bar{a}_2}(l))} \approx \frac{\bar{a}_2}{\bar{a}_1} \tag{14}$$

where mean$(\cdot)$ denotes average function. The validity of (14) has eliminated the influence of frequency. Therefore, when a set of intersection interval values under a particular $\bar{a}_1$ are known, the average value of the intersection interval values under the other $\bar{a}_2$ can easily be estimated.

III. OAM Switching Method Design and Results

A. OAM Switching Method Design

In the conventional VEMW radar forward-looking imaging model, the radar platform, equipped with a UCA, moves along the line of sight direction with a velocity v, forming a motion trajectory with a length denoted as L. The distance between the origin O and the imaging center is defined as R_s, which satisfies $\mathrm{L} \ll \mathrm{R}_s$. The azimuth echo from the imaging region can be expressed as follows [16]

$$\mathrm{S}(l,t) = \sigma_0 J_l^2(ka\sin\theta(t))e^{j2l\varphi_0} \tag{15}$$

where σ_0 represents the scattering coefficient of the target, $\theta(t)$ is the instantaneous elevation angle, φ_0 is the initial azimuth angle.

In the forward-imaging coordinate system, the instantaneous elevation angle can be expressed as [16]

$$\theta(t) \approx \theta_0 + \frac{\mathrm{v}t}{\mathrm{R}_0 \sin\theta_0} \tag{16}$$

where R_0 is the initial slant range, θ_0 is the initial elevation angle.

For the convenience of expression, K_a is introduced to represent the change rate of the elevation angle

$$\mathrm{K}_a = \frac{\mathrm{v}}{\mathrm{R}_0 \sin\theta_0} \tag{17}$$

Among the radar parameters, the duration of a single pulse is very short, and thousands or even more can be emitted in one second. As can be seen from (17), K_a is small, and θ does not change much within a few pulses. The black dotted line in Fig. 2 represents the first non-zero intersection of the adjacent order Bessel function. Combined with Fig. 2, it can be seen that if pulse-by-pulse method are used to transmit different OAM modes, when the elevation angle changes slowly, the radar beam energy in the ROI direction will drop sharply.; if a fixed OAM mode is used, the elevation angle between the radar and the target will slowly increase over time, which will cause the beam to shift and the echo energy in the ROI area will be weakened. Therefore, it is very necessary to design a reasonable OAM mode switching method to improve the SNR of the echo. According to the properties of the Bessel function intersection introduced in Section II-B, this section designs a method for OAM mode switching over time. The switching moment is approximately close to the energy of the l-order OAM beam being equal to the energy of the $(l+1)$-order OAM beam. According to the properties of the Bessel function intersection and the law of the elevation angle change between the radar and the target, the designed mode switching method is as follows

$$l(t) = l_{ini} + \lfloor \mathrm{f}_l t \rfloor \tag{18}$$

where $l(t)$ is the function that switches OAM mode over slow time, l_{ini} represents the initial transmitted OAM mode, and f_l represents the OAM mode switching rate.

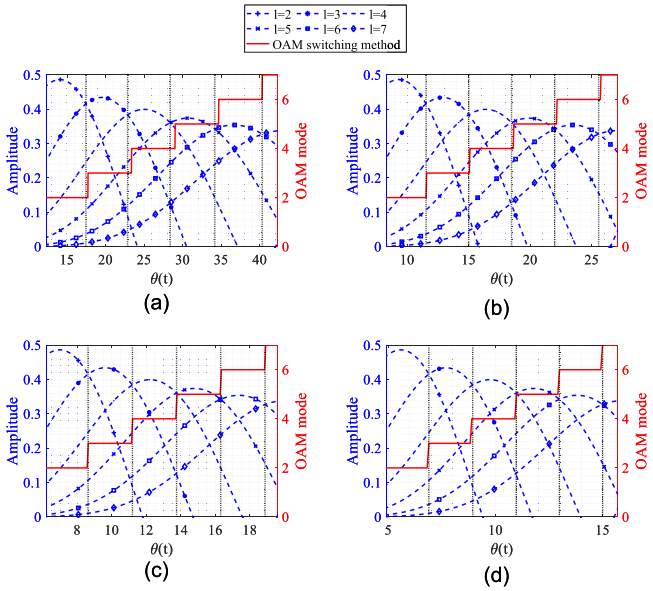

Fig. 2. The mode switching function designed according to different electrical size radii. (a)$\bar{a}=2$. (b)$\bar{a}=3$. (c)$\bar{a}=4$. (d)$\bar{a}=5$.

According to the initial position of the ROI and the radar system parameters, it is easy to calculate f_l

$$\mathrm{f}_l = \mathrm{K}_a / \mathrm{mean}(\alpha_{\bar{a}}(l)) \tag{19}$$

Fig. 2 shows the results obtained by designing the OAM mode switching method for different electrical size radii $\bar{a}$. As can be seen from the Fig. 2, the OAM mode switching moment is close to or coincident with the intersection of the adjacent OAM modes of the VEMW, and by comparing the sub-graphs in Fig. 2, it can be seen that as the $\bar{a}$ increases, the OAM mode switching moment proposed in this letter becomes more accurate, but in the case of a small $\bar{a}$, the switching error is less than 5%, which is acceptable. This design can effectively improve the energy utilization of each mode and increase the echo intensity of the ROI during the observation time.

To better understand this OAM mode switching method, we introduce a concept named OAM mode repetition frequency (OMRF), which represents the number of OAM modes transmitted per second. Since the variations in the elevation angle between the antenna and the target induced by OAM mode switching are significantly greater than those resulting from adjacent pulse intervals, the OMRF is considerably lower than the pulse repetition frequency (PRF). Therefore, multiple pulses are transmitted during the duration of a single OAM mode.

$$\mathrm{OMRF} = \mathrm{f}_l \tag{20}$$

In the actual imaging scenario, the azimuth echo containing noise can be expressed as

$$S_r(t) = \sum_{m=0}^{\mathrm{M}} \sigma_m J_{l(t)}^2(ka\sin\theta(t))e^{j2l\varphi_m} + n(t) \tag{21}$$

where $\mathrm{m} = 1, 2, 3, \ldots, \mathrm{M}$ represents the number of scatter points, $n(t)$ is Gaussian white noise with variance σ^2. Since

TABLE I
ENERGY ACCUMULATION OF DIFFERENT OAM MODE SWITCHING METHODS UNDER THE CONDITIONS OF V = 60M/S, PULSE DURATION TIME=10 μS, AND OBSERVATION TIME=1S

	The proposed method	Method A [16]	Method B [18]
$\bar{a}$=2	1963.1^2	1415.2^2	1026.4^2
$\bar{a}$=3	2035.2^2	1573.6^2	1118.3^2
$\bar{a}$=4	2246.1^2	1721.5^2	1341.6^2
$\bar{a}$=5	2194.3^2	1896.4^2	1423.1^2

the OAM mode of the VEMW satisfies the Fourier duality relationship with the azimuth angle, the azimuth angle information can be obtained by performing a fast Fourier transform (FFT) on the OAM mode domain of the obtained echo. According to the properties of FFT, the power of the echo without noise and noise after FFT is

$$\xi_{S(t)} = \sum_{t=0}^{\mathrm{L}/(v/\mathrm{PRF})} \left|S^2(t)\right| = \sum_{l_{ini}}^{l(t)} \int_{t}^{t+\mathrm{OMRT}} J_l^2(ka\sin\theta(t))dt \tag{22}$$

$$\xi_{n(t)} = \sigma^2 \tag{23}$$

where $\mathrm{OMRT} = 1/\mathrm{OMRF}$ is the OAM mode duration time. Therefore, the SNR can be expressed as

$$\mathrm{SNR} = 10 \cdot \log_{10}\left(\frac{\xi_{S_r(t)} - \xi_{n(t)}}{\xi_{n(t)}}\right) = 10 \cdot \log_{10}\left(\frac{\xi_{S(t)}}{\xi_{n(t)}}\right) \tag{24}$$

Since the designed OAM mode switching method can ensure that the ROI is in the maximum energy area of the current OAM mode at every moment, the power of the useful signal of the echo will be greatly improved, and the SNR of the ROI will also be improved [17]. This design greatly improves the anti-noise ability of the radar system and offers great potential in a low SNR environment.

B. Results

To make a simple comparison of energy utilization, the energy accumulated per unit time by the proposed method is compared with that of other methods under the same observation time and the same pulse duration.

From the data in Table I, it can be calculated that the method proposed in this letter improves energy by an average factor of 1.6595 compared to the time-sharing multi-mode transmitted method [18] and by an average factor of 3.0375 compared to the pulse-by-pulse switching mode transmitted method [16]. According to (24), it can be known that in theory [19], the proposed method can achieve the same effect when the SNR is 4.825 dB lower than the pulse-by-pulse switching mode method.

The improvement of energy is conducive to improving the imaging effect under low SNR, and can more accurately detect targets in low SNR imaging results.

Let the linear frequency modulation signal bandwidth transmitted by the radar is 50 MHz, the carrier frequency is 9.6 GHz, the pulse width is 10 μs, the antenna radius is 2λ, and the OAM mode used is [1,10]. The range information is obtained by using pulse compression on the range echo, and the azimuth information is obtained by using FFT on the OAM mode domain. The resolution in the range direction depends on the signal bandwidth, and the azimuth resolution δ_a depends on the number of effective OAM modes, i.e., $\delta_a \propto 2\pi/l_{effective}$.

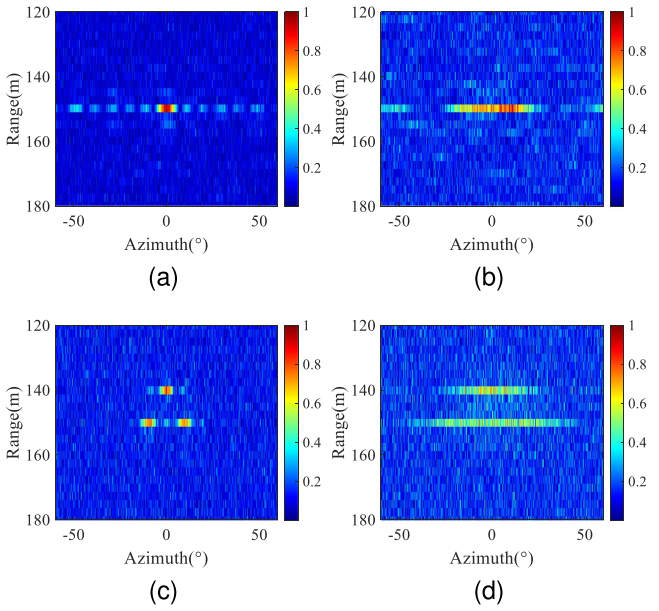

Fig. 3. (a) and (b) are the single-point target imaging results of the proposed method and the pulse-by-pulse OAM mode switching method at −10 dB, respectively. (c) and (d) are the multi-point target imaging results of the proposed method and the pulse-by-pulse OAM mode switching method at −20 dB, respectively.

Fig. 3(a) and (b) are the imaging results when −10 dB Gaussian white noise is added. It can be seen that the intensity of the target center reconstructed by the proposed method is higher than that by changing the transmitted mode pulse by pulse, which shows that the proposed method effectively improves the anti-noise performance of the radar system, and by comparing Fig. 3(a) and (b), it can be clearly seen that the azimuth resolution is improved. This is because the proposed method fully utilizes more OAM modes and increases the number of effective modes. At the same time, an experiment with a multi-point target SNR of −20 dB was set up. The results are shown in Fig. 3(c) and (d). It can be seen that the proposed method can distinguish the three targets well, while the comparison method has aliasing due to its low azimuth resolution. This result shows that the proposed method can still maintain good performance when the SNR is reduced.

IV. CONCLUSION

In conclusion, an approximate property of the adjacent-order Bessel functions is investigated. Subsequently, to ensure the maximum energy of the ROI, an OAM mode switching method is designed for making the most use of the energy of the OAM beams. Finally, by applying it to VEMW radar forward-imaging, the azimuth resolution and anti-noise ability are effectively improved. The method proposed in this letter provides a new way for OAM mode switching and has great application prospects. In the future, outdoor experiments will be carried out to further verify the proposed method.

REFERENCES

[1] L. Allen, M. W. Beijersbergen, R. Spreeuw, and J. Woerdman, "Orbital angular momentum of light and the transformation of Laguerre-Gaussian laser modes," *Phys. Rev. A*, vol. 45, no. 11, 1992, Art. no. 8185.

[2] S. M. Mohammadi et al., "Orbital angular momentum in radio—A system study," *IEEE Trans. Antennas Propag.*, vol. 58, no. 2, pp. 565–572, Feb. 2010.

[3] T. Yuan, Y. Cheng, H. Wang, and Y. Qin, "Mode characteristics of vortical radio wave generated by circular phased array: Theoretical and experimental results," *IEEE Trans. Antennas Propag.*, vol. 65, no. 2, pp. 688–695, Feb. 2017.

[4] Y. Chen et al., "A flat-lensed spiral phase plate based on phase-shifting surface for generation of millimeter-wave OAM beam," *IEEE Antennas Wireless Propag. Lett.*, vol. 15, pp. 1156–1158, 2016.

[5] Y. Wang, Q. Guo, J. Xiang, and Y. Zhong, "Millimeter-wave MIMO transmission for FBMC systems with lens antenna arrays," *IEEE Signal Process. Lett.*, vol. 32, pp. 1141–1145, 2025.

[6] F. Shen, J. Mu, K. Guo, S. Wang, and Z. Guo, "Generation of continuously variable-mode vortex electromagnetic waves with three-dimensional helical antenna," *IEEE Antennas Wireless Propag. Lett.*, vol. 18, no. 6, pp. 1091–1095, Jun. 2019.

[7] S. Yu, L. Li, G. Shi, C. Zhu, and Y. Shi, "Generating multiple orbital angular momentum vortex beams using a metasurface in radio frequency domain," *Appl. Phys. Lett.*, vol. 108, no. 24, 2016, Art. no. 241901.

[8] Z. Lu, J. Wang, J. Lian, and Y. Wang, "A mode-matching approach for acoustic vortex generation in circular array configurations," *IEEE Signal Process. Lett.*, vol. 31, pp. 1590–1594, 2024.

[9] M. Lin, Y. Gao, P. Liu, and J. Liu, "Theoretical analyses and design of circular array to generate orbital angular momentum," *IEEE Trans. Antennas Propag.*, vol. 65, no. 7, pp. 3510–3519, Jul. 2017.

[10] K. Liu et al., "Generation of OAM beams using phased array in the microwave band," *IEEE Trans. Antennas Propag.*, vol. 64, no. 9, pp. 3850–3857, Sep. 2016.

[11] H. Qu, S. Li, C. Chen, J. Liu, and W. Chen, "High-resolution orbital angular momentum imaging with the removal of Bessel function modulation effect," *IEEE Trans. Microw. Theory Techn.*, vol. 72, no. 4, pp. 2577–2590, Apr. 2024.

[12] H. Qu, C. Chen, J. Liu, and W. Chen, "Enhanced vortex wavefront modulated radar forward-looking variational Bayesian hierarchical structural sparse imaging by leveraging the continuity of target scene," *IEEE Trans. Aerosp. Electron. Syst.*, vol. 61, no. 3, pp. 5962–5979, Jun. 2025.

[13] T. Zhou, Z. He, Q. Shi, C. Lin, and S. Zhang, "Multisnapshot high-resolution gridless DOA estimation for uniform circular arrays," *IEEE Signal Process. Lett.*, vol. 31, pp. 1705–1709, 2024.

[14] T. Yuan, Y. Cheng, H. Wang, and Y. Qin, "Beam steering for electromagnetic vortex imaging using uniform circular arrays," *IEEE Antennas Wireless Propag. Lett.*, vol. 16, pp. 704–707, 2017.

[15] F. W. J. Olver and L. C. Maximon, "NIST digital library of mathematical functions: Chapter 10 Bessel functions," National Institute of Standards and Technology, May 2025. Accessed: May 2025. [Online]. Available: https://dlmf.nist.gov/10

[16] H. Pan, H. Ma, D. Hu, and H. Liu, "Novel forward-looking three-dimensional imaging based on vortex electromagnetic wave radar," *J. Radars*, vol. 13, pp. 1109–1122, 2024.

[17] L. Tian, C. Xu, D. Chen, D. He, and T.-K. Truong, "Enhancing mmWave DOA estimation by cumulative power gradient at low SNR," *IEEE Signal Process. Lett.*, vol. 27, pp. 1974–1978, 2020.

[18] J. Wang, K. Liu, H. Liu, K. Cao, Y. Cheng, and H. Wang, "3-D object imaging method with electromagnetic vortex," *IEEE Trans. Geosci. Remote Sens.*, vol. 60, 2022, Art. no. 2000512.

[19] Q. Zhang, Z. Li, L. Yu, and Z. Dong, "A quantitative SNR analysis for the adjacent cross correlation function," *IEEE Signal Process. Lett.*, vol. 30, pp. 1192–1196, 2023.